

## EXAFS Spectroscopy by Continuum Soft X-ray Emission from a Short Pulse Laser-produced Plasma

G. J. Tallents,<sup>A,B</sup> B. Luther-Davies<sup>A</sup> and M. A. Horsburgh<sup>C</sup>

<sup>A</sup> Laser Physics Laboratory, Department of Engineering Physics,  
Research School of Physical Sciences, Australian National University,  
G.P.O. Box 4, Canberra, A.C.T. 2601.

<sup>B</sup> Present address: JET Joint Undertaking, Abingdon, OX14 3EA, U.K.

<sup>C</sup> Department of Physical Chemistry, School of Chemistry,  
University of Sydney, Sydney, N.S.W. 2006.

### Abstract

The use of a laser-produced plasma created by low energy ( $E \leq 6$  J), ps duration laser pulses as the X-ray source for EXAFS spectroscopy in the 3-8 Å wavelength band is investigated. We consider the various factors that affect the X-ray flux at the detector plane and investigate ways of optimizing that flux. A simple qualitative model has been used to describe the way in which the source intensity scales with parameters such as the laser intensity. Practical problems associated with the implementation of the various different X-ray dispersive elements and detectors are discussed.

### 1. Introduction

Laser-produced plasmas are under investigation as sources of continuum X-ray emission for studies of the absorption spectra of materials (Mallozi *et al.* 1979, 1981; Epstein *et al.* 1983; Eason *et al.* 1984). Measurement of the wavelengths of absorption edges and the recording of extended X-ray absorption fine structure (EXAFS) spectra and X-ray absorption near-edge structure (XANES) spectra are of current major interest in physical chemistry and solid state physics (Teo 1980; Pendry 1983). Laser-produced plasmas have some distinct advantages as X-ray sources for such absorption measurements, compared with the now traditional synchrotron sources, because they produce a very high flux of soft X-rays ( $10^5$ - $10^6$  that of a synchrotron when laser pulses of kJ energy are available) from an essentially point source on a timescale comparable with that of the laser pulse duration (down to a few tens of ps). As a laser-produced plasma is close to being a point X-ray source, the whole range of X-ray wavelengths can be recorded simultaneously and the short duration of the X-ray emission can be used for time-resolved absorption measurements (Forster *et al.* 1984). To-date high energy ( $\geq 100$  J) lasers designed for fusion research have been used almost exclusively for X-ray production research and there has been little attempt to optimize the experimental parameters to permit the use of lower energy systems. If laser-based sources are, however, to have an impact on EXAFS or XANES spectroscopy, it is highly desirable that smaller, high repetition rate lasers be used in order to reduce the cost and complexity of the systems and increase the data rate. In that case the laser-produced plasma X-ray source would

be inexpensive to build and operate in comparison with a synchrotron and would open up the possibility of in-house X-ray facilities when synchrotron sources were unavailable.

With this in mind, in the present paper we have studied the production of continuum emission from a laser-produced plasma in the wavelength range from 3 to 8 Å and investigated the practical limitations that the use of currently available X-ray diffraction crystals and X-ray detectors place on the development of a laser EXAFS system using a monojoule laser source. By optimizing the X-ray emission and spectrograph sensitivity, we have recorded EXAFS spectra using a single, short duration ( $\sim 150$  ps), low energy ( $< 6$  J) phosphate glass laser pulse to generate a plasma X-ray source. In our geometry, plasmas created by slightly defocused pulses of short wavelength laser radiation are shown to produce the greatest X-ray flux. The three types of crystal spectrograph that have been investigated (plane, Von Hamos and elliptical) have been recently reviewed (Yaakobi *et al.* 1979; Yaakobi and Burek 1983; Henke *et al.* 1983). It is shown that the cylindrically bent Von Hamos spectrograph gives the most sensitive detection threshold for X-rays, while still providing high dispersion.

## 2. Method

### (a) Laser-produced Plasma X-ray Source

The phosphate glass laser used for these experiments produces a maximum energy of between 3–6 J in a single pulse of duration between 20 and 200 ps at a wavelength of 1.054  $\mu\text{m}$ . The beam was focused onto solid targets by using a high quality  $f/1$ , 110 mm aperture lens which produces a near diffraction limited focal spot with an in-vacuum focal diameter of 2  $\mu\text{m}$  at half-intensity. When the pulse duration is 20 ps, the maximum laser energy is 3 J and the peak vacuum laser intensity  $\sim 10^{18}$   $\text{W cm}^{-2}$ . Correspondingly lower peak intensities are obtained with longer pulses, although the energy which can be produced increases to  $\approx 6$  J for pulses longer than 80 ps. Some experiments are reported in this paper where output from the laser was frequency-doubled to produce radiation at a wavelength of 0.53  $\mu\text{m}$ . The maximum energy obtained in this configuration was  $\approx 1$  J due to the limited aperture of the frequency doubling crystal.

The laser was focused onto plane foil targets with the target normal at angles between  $0^\circ$  and  $30^\circ$  to the axis of the laser beam. Mead *et al.* (1981, 1983) found that the absorption of laser light by the target is constant over this angular range. Measurements of the volume-averaged and time-averaged temperatures created in the laser-produced plasmas have been made by using an 11-channel X-ray spectrometer array with silicon photodiode detectors (Burgess *et al.* 1983). It was found that the 'thermal' temperatures characterizing the electron energy distribution of the bulk of the plasma electrons are typically  $\approx 500$  eV for laser pulses of 20 ps duration and wavelength 1.054  $\mu\text{m}$ . The thermal temperatures vary only very slowly with target position (i.e. laser intensity) relative to the position of the best focus and are also almost totally independent of the laser energy. A small fraction ( $< 1\%$ ) of the electrons in the plasma have an energy distribution which can be characterized by a much higher 'superthermal' temperature. The superthermal temperature increases with increasing laser intensities (ranging from a few to a few tens of keV for intensities in the range  $10^{14}$ – $10^{16}$   $\text{W cm}^{-2}$ , see Burgess *et al.* 1983), but the X-ray emission

generated by these superthermal electrons forms only a minor portion of the X-ray signal for wavelengths greater than 3 Å. However, they do produce sufficient hard X-rays to cause X-ray fluorescence in apparatus close to the target and consequent 'fogging' of the X-ray detectors.

The duration of soft X-ray emission from the laser-produced plasma has been measured by means of an X-ray streak camera (Hadland Photonics X-chron) with a gold coated beryllium photocathode located about 200 mm from targets irradiated with laser pulses of energy 3 J and duration 200 ps. The X-rays reaching the photocathode were filtered at different positions across the streak camera slit, by 125 μm thick Be, 9 μm thick Fe and 6.35 μm thick Ni filters, to select different X-ray bands in the 2–6 Å region. Within the resolution and dynamic range of the streak camera (approximately 15 ps and 100 respectively) and, providing that there are no strong spectral lines present in the soft X-ray spectrum, the duration of the X-ray emission was found to match that of the laser pulse.

The fraction of laser energy absorbed by the plasma has been measured with a box calorimeter surrounding the laser-produced plasma (Perry 1986) and was found to vary only slowly with laser energy and intensity. Typically, about 30% of the laser energy is absorbed by the target when the target is closer to the lens than the best focusing position for the lens, and about 20% is absorbed when the target is further from the lens than the best focus position. By using multi-layered targets and monitoring the  $K_{\alpha}$  fluorescence generated by high energy electrons that penetrate to an element placed on the rear of the targets, we have also established that about 10% of the absorbed energy is carried by the superthermal electrons whose characteristic temperature reaches 80 keV for an intensity  $I_0 > 3 \times 10^{17} \text{ W cm}^{-2}$ . A lower limit can be placed on the magnitude of the X-ray signal in the lower wavelength range 0.15–3 Å generated by these superthermal electrons by simply characterizing them as a current pulse of high energy electrons generating bremsstrahlung from within a cold solid target. The peak electron current is about 10 kA with the average electron energy up to 80 keV. The peak power emitted as hard X-ray continuum, therefore, exceeds that available from many conventional X-ray tubes (Germer 1979) by about six orders of magnitude and is comparable with that available from the current generation of synchrotrons. However, any advantage a low energy laser X-ray source will have over X-ray tube and synchrotron sources in the hard X-ray region will clearly rely on very efficient utilization of the available flux and the development of high repetition rate lasers that permit signal averaging or integration.

### *(b) Crystal Spectrographs*

A complete laser-EXAFS system will consist of the source, whose basic characteristics have been described above, a sample which is 'probed' by the continuum emission generated by the plasma, a dispersive element to split the X-ray beam transmitted by the sample into its wavelength components and a detection system. The simplest form of dispersive element is a plane crystal spectrograph (see Fig. 1a). It offers the advantage of ease of manufacture and avoids the necessity to choose diffracting crystals which can be bent. However, it does have an inherently low collection efficiency which can only be improved by placing the crystal very close to the source and this can place unacceptable physical restrictions on the experimental geometry. We have, however, recorded spectra with a plane spectrograph using an

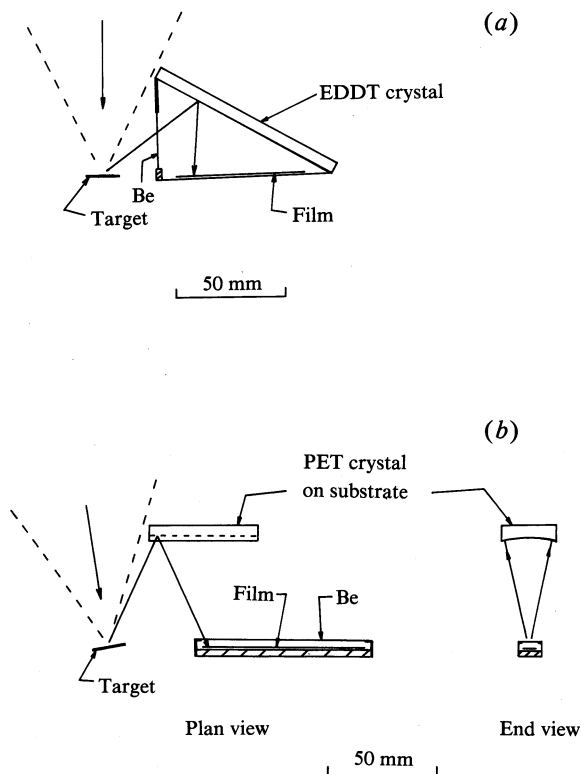


Fig. 1. Schematic diagrams of (a) the plane crystal spectrograph and (b) the Von Hamos spectrograph. Possible paths of X-rays with a wavelength equal to the wavelength of the K-edge of aluminium ( $7.95 \text{ \AA}$ ) are shown by straight arrows.

Table 1. Crystals used in the plane and Von Hamos spectrographs

Crystal (Reflection plane)	$2d$ ( $\text{\AA}$ )	Spectrograph type	Minimum radius of curvature (mm)
EDDT (020)	8.808	Plane	Not bent
Mica (002)	19.92	Von Hamos	50
PET (002)	8.742	Von Hamos	50

Table 2. Integrated reflectivity of crystals

Results are taken from Gould *et al.* (1968) and Gilfrich *et al.* (1975)

$\lambda$ ( $\text{\AA}$ )	Integrated reflectivity ( $10^{-5}$ rad)			Graphite
	EDDT	Mica	PET	
1.54	$\sim 22$		41	220
2.75		2.6	22	120
4.73	4.1	2.7		49
5.37	5.1	2.5	11	59
6.16	3.6	2.1		77
7.13		2.9	13	

EDDT (ethylene diamine dihydrogen tartrate) crystal (see Table 1). Around 50 laser pulses, each of 2 J, were needed to obtain sufficient film exposure to record aluminium K-edge EXAFS spectra (see Section 3). Some improvement in the performance of the plane crystal device can be expected by using crystals with a higher diffraction efficiency. Pentaerythritol (PET) offers improvement over EDDT by a factor of two, whilst pyrolytic graphite is an even better choice with its integrated reflectivity exceeding that of EDDT by about one order of magnitude (see Table 2). Even with these improved materials, however, single shot exposures would not be possible with only 1–2 J of laser energy at the 1  $\mu\text{m}$  neodymium or phosphate glass laser wavelength although, as is evident from the results of Section 3a, by frequency multiplying the laser output, single shot exposures would probably be obtainable near the aluminium K-edge (7.95  $\text{\AA}$ ).

An elliptically bent crystal spectrograph (Henke *et al.* 1983) was also built and tested. The elliptical design has some advantages for EXAFS spectroscopy. The dispersion can be made arbitrarily large or small, depending on the radius of curvature chosen for the film plane and X-rays of all wavelengths pass through a narrow slit area which can be used to hold a small sample of material in order to obtain the EXAFS spectrum of that material (see Henke *et al.* 1983). However, there is no focusing of the X-rays in the non-dispersive direction and hence it is necessary to have a small dispersion and a small ellipse which must be positioned close to the target in order to have reasonable detection sensitivity. We found that it was very difficult to bend PET crystals to conform to the elliptical substrates for small (minor axis <50 mm) ellipses (though this is possible with mica). As a result, the elliptical spectrograph sensitivity is relatively low and does not exceed that of the cylindrical Von Hamos geometry crystals discussed below.

The Von Hamos spectrograph design (see Fig. 1b) enables a greater detection sensitivity than the plane or elliptic spectrographs as X-rays from a large solid angle are concentrated into a line focus with the wavelengths dispersed along the line. The magnitude of the dispersion is a function of the radius of curvature of the crystal, whilst the fact that the source and image planes are equidistant from the crystal makes it possible to use the full rocking angle of the crystal without loss of resolution (Yaakobi and Burek 1983). The major problem with the Von Hamos geometry is that the diffracting crystal must be accurately bent. We have used mica (muscovite) and PET as the diffracting crystal in this geometry (see Table 1). Both in-house and commercially bent crystals have been used, but both have provided relatively poor line foci. Nevertheless, the width of the focal line was 1–2 mm which resulted in more than one order of magnitude more flux density at the film plane than for a comparable plane crystal. The focus was, however, highly striated and hence analysis of data recorded on film was inaccurate. With a better quality bent crystal and a detector capable of integrating over the width of the focus, considerably better performance should be achievable. Comparison of, for example, a plane and bent crystal with the same dispersion shows that the Von Hamos geometry can provide greater flux in the recording plane by a factor of 100 (Yaakobi *et al.* 1979).

The in-house bent crystals were made by cleaving mica or PET to very thin (10–20  $\mu\text{m}$ ) sheets by using razor blades. The crystal sheets were then made to conform to the substrate by suction. Substrates with many small (0.5 mm diameter) surface holes inter-connected to a vacuum and ballast system were found to produce the best conformed crystals. A secondary system of small surface holes into which

a slow drying contact glue (e.g. Loctite penetrating adhesive) can be dropped from the back of the substrate to fix the crystal onto the substrate is also useful. However, even crystals mounted in this way were found to conform relatively poorly to the shape of the substrate and unfortunately, several months after manufacture, the PET crystals bent to tight radii (e.g. 50 mm) and tended to cleave and bulge in places.

In our experiments, the Von Hamos spectrograph was aligned relative to the target position with a thin (20  $\mu\text{m}$  diameter) optical fibre carrying a helium–neon laser output. An end of the fibre was positioned at the focal position of the laser focusing lens and the spectrograph aligned relative to the light emitted from the optical fibre. As the light from the end of the optical fibre comes from an area of similar or smaller size than the laser-produced plasma X-ray emission area, we found that the Von Hamos spectrograph can be accurately focused for X-rays using the visible light from the optical fibre.

### (c) Detection

We have measured the flux in the detector plane from a PET Von Hamos spectrograph. A slit placed on the focal line selected a narrow range of X-ray wavelengths behind which was positioned an absolutely calibrated (Hohlfelder 1974) silicon X-ray photodiode. A beryllium filter of thickness 25  $\mu\text{m}$  was used to stop ultra-violet and visible light from exposing the photodiode. As well as giving an absolute measure of the X-ray flux diffracted from the crystal, the use of a photodiode allows quick monitoring of the variation of X-ray emission with parameters such as laser energy and intensity (see Section 3). The height of the slit was about 3 mm which allowed collection of X-rays from the whole width of the focal region.

Ceaverken Reflex 25 X-ray film was usually used to record the whole X-ray spectrum with beryllium filters again being used to prevent scattered laser and plasma light from reaching the film. The X-ray film was developed for 4 min in Kodak liquid X-ray developer at 20° C, placed in a stop-bath of 5% acetic acid solution for 30 s and then fixed for 4 min in Kodak liquid X-ray fixer. The film was washed after fixing for at least 30 min and the optical densities of exposures measured with a Joyce–Loebl densitometer.

The Ceaverken film has been checked to have a linear optical density response with exposure over a wide optical density range. Poorly bent crystals used in the Von Hamos spectrograph tend to produce many striations instead of a single focal line. A spectral line emitted from the laser-produced plasma was thus recorded with several optical densities, one for each striation. We have constructed a curve showing the optical density for spectral lines in a ‘dense’ striation  $D_{\text{high}}$  as a function of the optical density of the same spectral lines in a ‘low density’ striation  $D_{\text{low}}$  (see closed circles in Fig. 2). Fig. 2 also shows data for (i) the recorded optical density jumps from the high to the low wavelength side of the K-edge of aluminium as a function of the optical density expected on the low wavelength side of the K-edge because of the known attenuation (diamonds) and (ii) the optical density of different spectral lines in a five shot exposure compared with their optical density in a single shot (open circles). Data for (i) and (ii) have been scaled in the manner outlined by Tallents and Shorrock (1981) and Lewis and Mahoney (1984) to coincide with the ‘dense’ striation/‘less dense’ striation comparison. Altogether, providing we assume that low optical density exposures (for example, where  $D < 0.4$ ) have the optical density  $D$  proportional to the exposure (not an unreasonable assumption,

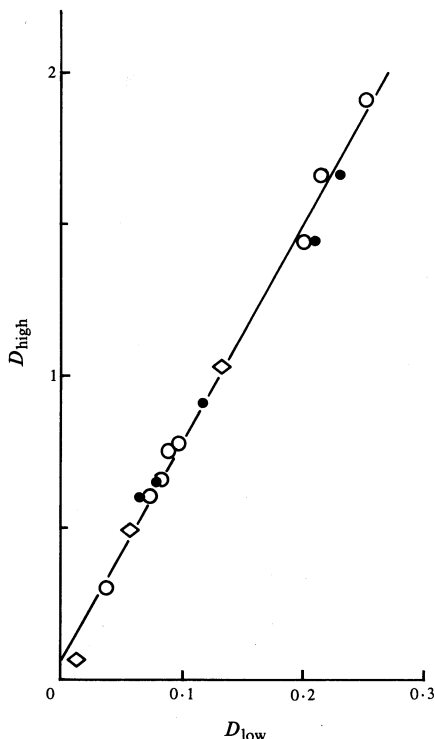


**Fig. 2.** Linear optical density response of Ceaverken Reflex 25 X-ray film with exposure showing

- optical densities recorded for the aluminium He-like line  $1s^2\ ^1S_0-1s2p\ ^1P_1$  and satellites to this line in 'dense' (ordinate) and 'less dense' (abscissa) striations of a poorly focused Von Hamos spectrograph (see text);
  - ◇ recorded optical density jumps (ordinate) from the high to the low wavelength side of the K-edge of aluminium as a function of the optical density expected on the low wavelength side because of the known attenuation;
  - optical densities of the aluminium He-like line  $1s^2\ ^1S_0-1s2p\ ^1P_1$  and satellites in a five shot (ordinate) and a single shot (abscissa) exposure;
  - least-squares fit to data points.
- Points ◇ and ○ are scaled horizontally to coincide with ● (see text).

see Dozier *et al.* 1976; Tallents and Shorrock 1981), the results of Fig. 2 show that the optical density is proportional to exposure for  $D < 2$ .

### 3. Results

#### (a) Continuum Emission

Fluxes of X-ray continuum were recorded using a Von Hamos spectrograph with a 50 mm radius of curvature PET diffracting crystal of dimensions 25 by 50 mm (width by length), for an X-ray wavelength range of  $0.017\ \text{\AA}$  centred on  $4.8\ \text{\AA}$ . Fig. 3 shows the flux of X-ray continuum as a function of laser energy for a lead target irradiated by laser pulses of 130 ps and wavelength  $1.054\ \mu\text{m}$ . The X-rays were recorded by means of the silicon photodiode with the wavelength range selected by a slit on the focal plane (see Section 2c). From a least-squares fit to the experimental data in Fig. 3 we found that the X-ray flux  $F$  varies approximately with the laser energy  $E$  as  $F \propto E^{1.6}$ . Using this proportionality to normalize the X-ray flux to the value expected for a laser energy of 2 J, we obtained the variation of X-ray flux with target position relative to the laser focus (Fig. 4). The largest flux of X-rays are emitted for a target position  $150\ \mu\text{m}$  closer to the focusing lens than the position of best focus for the lens (Fig. 4). The X-ray flux with the target positioned  $150\ \mu\text{m}$  further from the focusing lens than the position of best focus for the lens also peaks, but with less emission, probably correlating with the smaller laser absorption in the plasma observed for such 'negative' focal positions (Perry 1986). The relative efficiency of X-ray production as a function of the peak intensity of the laser light at the target surface is shown in Fig. 5. The results of Figs 3–5 are interpreted in terms of a simple model of X-ray production in Section 4a.

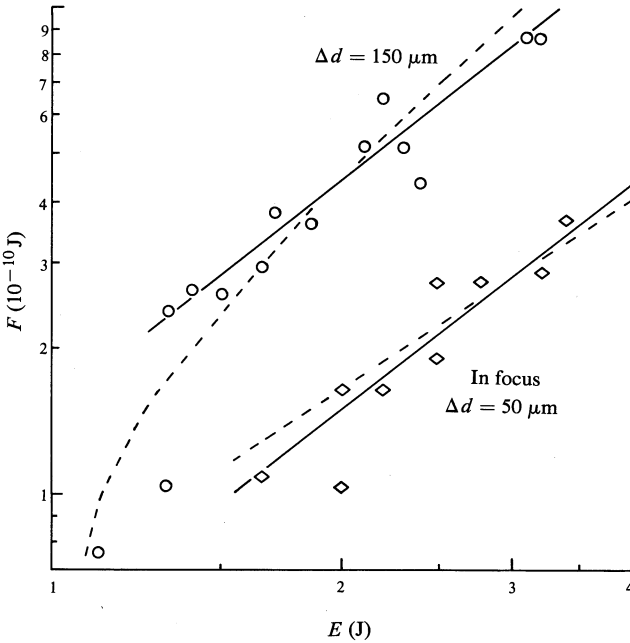


Fig. 3. Flux  $F$  of X-ray energy as a function of laser energy  $E$  for a target in the position of the laser focus and  $150\ \mu\text{m}$  closer to the lens. Results are for a lead target (with the target normal at  $30^\circ$  to the laser axis) irradiated by laser pulses of 130 ps and wavelength  $1.054\ \mu\text{m}$ . Least-squares fits to data points are shown as solid lines. The expected variations of  $F$  according to equation (6) (Section 4*a*) with  $\Delta d = 50$  and  $150\ \mu\text{m}$  are shown as broken curves.

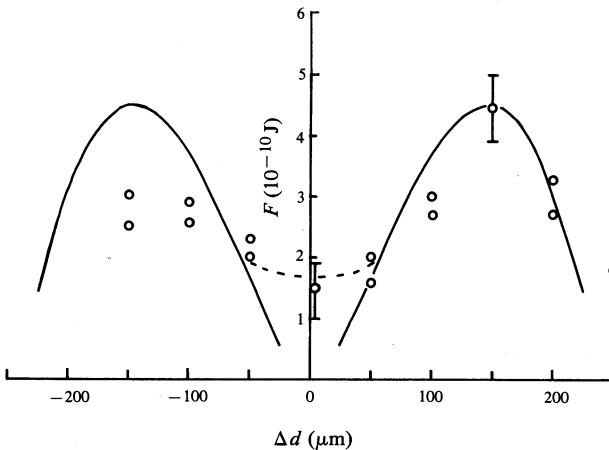
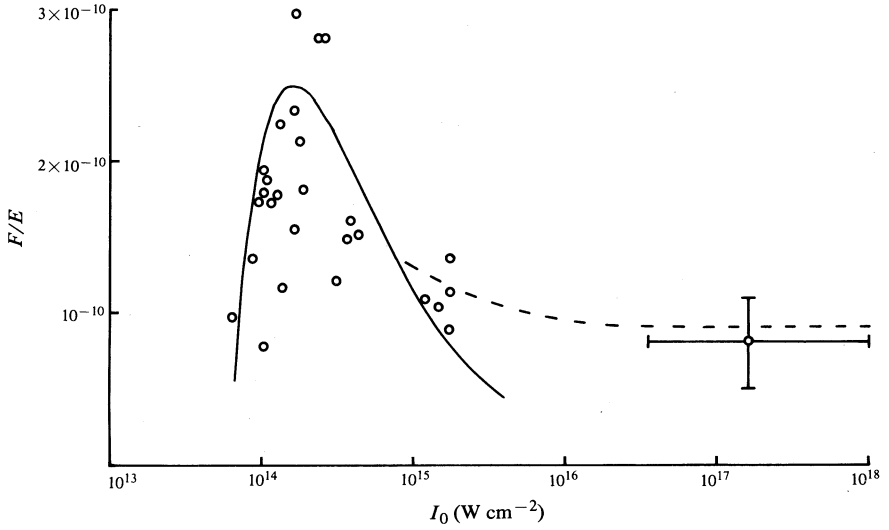
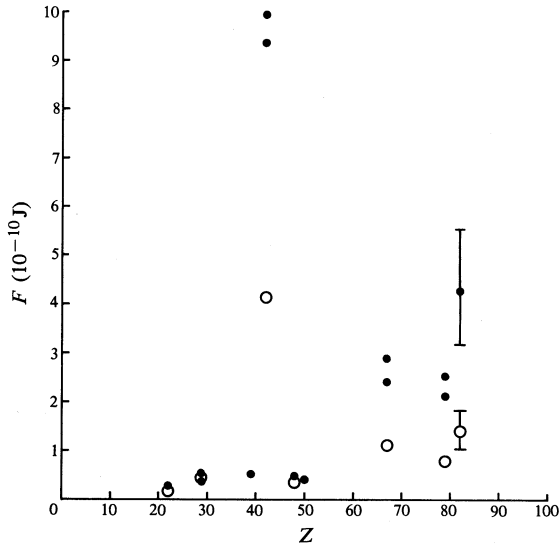


Fig. 4. Flux  $F$  of X-ray energy (normalized to the values expected for a laser energy of 2 J), as a function of the position  $\Delta d$  of the target relative to the laser focus. Negative values of  $\Delta d$  imply that the point of laser focus is in front of the target surface, while positive values imply that the point of laser focus is behind the target surface. Results are for the lead target described in Fig. 3. The expected variations of  $F$  according to equation (6) are shown as solid curves, with a broken curve indicating the effect of minimum plasma size as  $\Delta d \rightarrow 0$  (see Section 4*a*).



**Fig. 5.** Ratio of flux  $F$  of X-ray energy to laser energy  $E$  as a function of the peak laser intensity  $I_0$  at the target. Results are for the lead target described in Fig. 3. The expected variation of  $F/E$  according to equation (6) is shown as a solid curve, with a broken curve indicating the effect of the minimum plasma size as  $\Delta d \rightarrow 0$  and  $I_0$  increases (see Section 4a).



**Fig. 6.** Flux  $F$  of X-ray energy (normalized to the values expected for a laser energy of 2 J) as a function of the target atomic number  $Z$ . Results are for targets irradiated by laser pulses of 130 ps and wavelength  $1.054 \mu\text{m}$ . The closed circles are for a target position  $150 \mu\text{m}$  defocused from the laser focus, while the open circles are the results when the target is at the position of laser focus.

The soft X-ray emission from our laser-produced plasma tends to increase with target atomic number  $Z$  (Fig. 6). However, an exception to this flux increase with  $Z$  is the high X-ray flux from molybdenum ( $Z = 42$ ) targets due to some spectral lines and possibly some free-bound continuum covering the spectral range of our observations (see Fig. 7*a*). The X-ray flux at higher wavelengths, for example close to the K-edge of aluminium ( $7.95 \text{ \AA}$ ), shows similar variations with laser energy and target position to the results presented in Figs 3–6 for a wavelength of  $4.8 \text{ \AA}$ , although the X-ray flux is generally greater at higher X-ray wavelengths. The variation of X-ray emission with wavelength is shown in Fig. 7 for targets of molybdenum, gold and lead. From Fig. 7, we see that the continuum emissions recorded in the wavelength range  $3\text{--}7 \text{ \AA}$  are largely in wavelength bands and may be mainly a quasi-continuum of many broadened, closely spaced spectral lines (Busquet *et al.* 1985). Some identified molybdenum spectral lines in (*a*) are labelled with wavelengths deduced by Kallne *et al.* (1983) and some gold lines in (*b*) are labelled with wavelengths deduced by us (see also the recent work by Busquet *et al.* 1985 and Kiyokawa *et al.* 1985). Individual spectral lines cannot be seen in the lead spectrum (*c*).

Numerous authors have shown that frequency doubling the laser which creates the laser-produced plasma results in a greater X-ray emission from the plasma (Yaakobi *et al.* 1981; Mathews *et al.* 1983). From the Von Hamos spectrograph on X-ray film with four shots of  $\approx 1 \text{ J}$  laser energy focused onto gold targets using the doubled laser frequency ( $\lambda = 0.53 \text{ \mu m}$ ), we obtained similar exposures to those obtained with three shots of  $\approx 2.5 \text{ J}$  laser energy focused onto gold targets using the fundamental laser frequency ( $\lambda = 1.054 \text{ \mu m}$ ). From the X-ray flux dependence on laser energy obtained from Fig. 3, this means that for comparable laser energies the X-ray flux produced with the doubled laser frequency is greater than that produced with the fundamental laser frequency by a factor of  $\approx 3\text{--}4$ .

It has also been reported that the X-ray emission increases with laser pulse-length (see e.g. Epstein *et al.* 1983). Lengthening our laser pulse-length enables larger laser energies to be generated, but we found that for comparable laser energies the X-ray flux is constant with increasing laser pulse length over the pulse-length range  $20\text{--}200 \text{ ps}$ .

### (*b*) EXAFS Spectra

The EXAFS spectrum of the K-edge of aluminium recorded with a plane EDDT crystal spectrograph is shown in Fig. 8. An aluminium foil of  $2 \text{ \mu m}$  thickness was placed over the film in the spectrograph (see Fig. 1*a*) and 50 laser shots of  $20 \text{ ps}$  duration and energy  $2 \text{ J}$  focused onto a gold target were used to produce the X-rays for the EXAFS exposure (Fig. 8*b*). A 'control' exposure of the continuum emission from the gold plasma was produced (Fig. 8*a*) by 15 laser shots of  $20 \text{ ps}$  duration without the aluminium foil in place. The aluminium foil transmission shown in Fig. 8*c* was obtained by dividing the EXAFS exposure (*b*) by the emission exposure (*a*). Following the analysis by Mallozi *et al.* (1979), the wavelength spacing of the EXAFS peaks gives a nearest neighbour distance of  $2.66 \text{ \AA}$  in the aluminium foil. However, the method of analysis by Mallozi *et al.* (1979) gives inter-atom distances which are typically  $10\text{--}20\%$  shorter than their true values because the method neglects the phase changes experienced by the photo-electron in the absorption process (Eason *et al.* 1984). A phase change correction of  $+0.4 \text{ \AA}$  to the measured nearest-neighbour distance

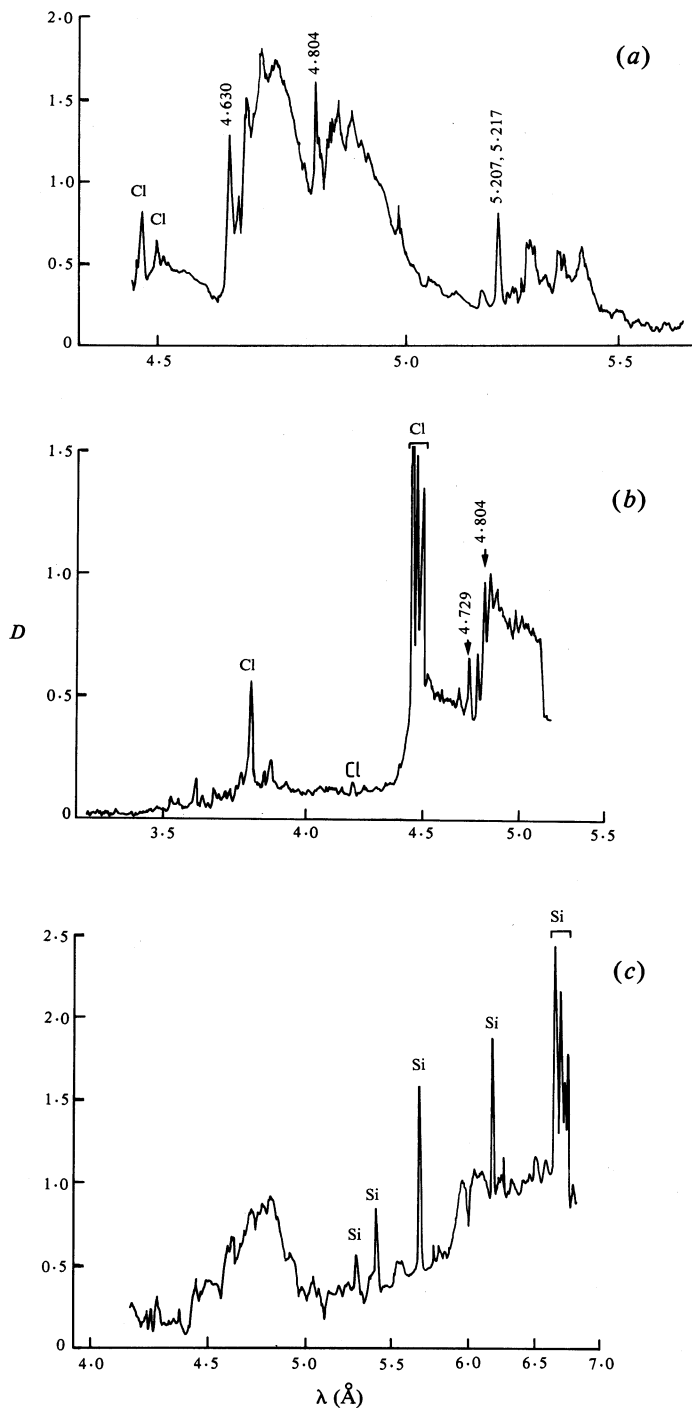


**Fig. 7.** Spectra of X-ray emission from the laser-produced plasma for targets of (a) molybdenum ( $Z = 42$ ), (b) gold ( $Z = 79$ ) and (c) lead ( $Z = 82$ ). The spectra for molybdenum and gold have chlorine lines due to the emission from a single laser shot onto Saran (polyvinylidene chloride) superimposed as a wavelength standard. For the same reason the spectrum for lead has silicon lines due to the emission from a laser shot onto glass.

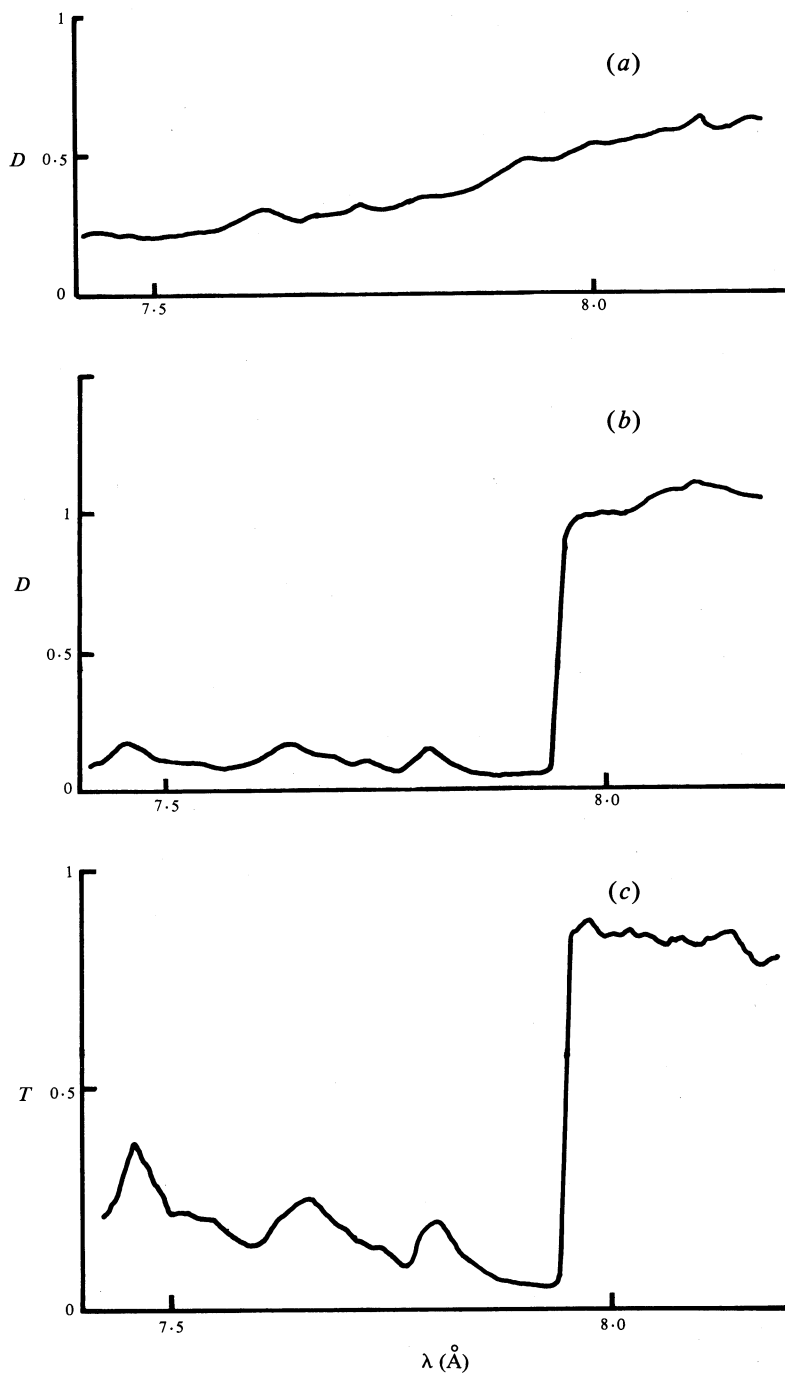


**Fig. 8.** The EXAFS spectrum of the K-edge of aluminium obtained with a plane crystal spectrograph. Plots show (a) recorded continuum emission from the laser-produced plasma; (b) absorption spectrum measured after X-rays have passed through a foil of  $2 \mu\text{m}$  thick aluminium; (c) foil transmission obtained by dividing (a) into (b) at each wavelength. Plot (b) required an exposure of 50 laser shots of  $\approx 2 \text{ J}$  per shot.

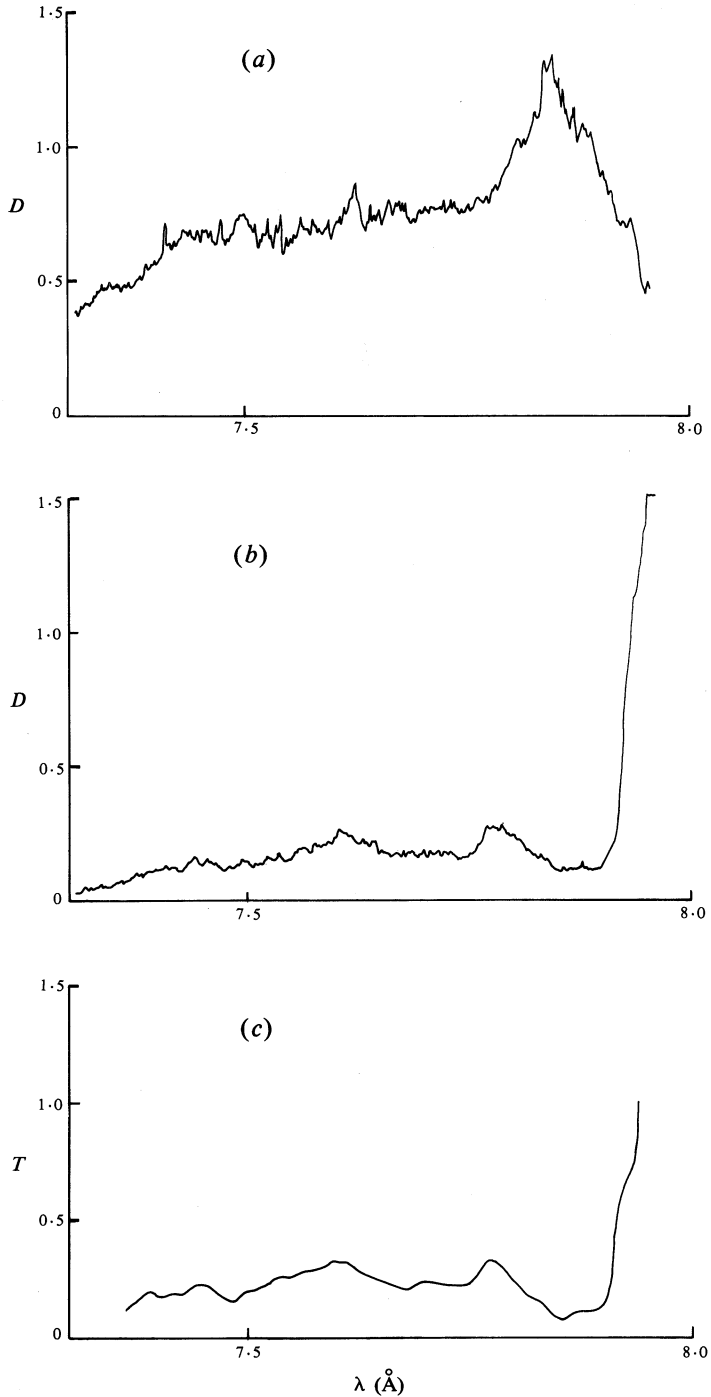


**Fig. 9.** The EXAFS spectrum of the K-edge of aluminium obtained with a Von Hamos crystal spectrograph. Plots show (a) recorded continuum emission from the laser-produced plasma; (b) absorption spectrum measured after X-rays have passed through a foil of  $0.75 \mu\text{m}$  thick aluminium; (c) foil transmission obtained by dividing (a) into (b) at each wavelength. The plot (b) required an exposure of one laser shot of  $5.5 \text{ J}$ .

has been calculated for aluminium (Fontaine *et al.* 1979), and hence our measured nearest-neighbour distance for aluminium is  $3.06 \text{ \AA}$ , in approximate agreement with the known nearest-neighbour distance of  $2.86 \text{ \AA}$  for the aluminium face-centred-cubic lattice.

The EXAFS spectrum (Fig. 8) illustrates the capabilities of laser-produced plasmas as X-ray sources, but clearly the plane crystal spectrograph used to obtain the spectrum is not suitable for more routine determinations of EXAFS because of the large number of laser shots required. We found, however, that by using a cylindrically bent Von Hamos spectrograph, it is possible to record single shot exposures with our laser-produced plasma source. The EXAFS spectrum of the K-edge of aluminium recorded in this way is shown in Fig. 9. An aluminium foil of  $0.75 \text{ }\mu\text{m}$  thickness was placed over the film and a single laser shot of 100 ps duration and energy  $5.5 \text{ J}$  focused onto a gold target was used as the X-ray source. By using the method of analysis by Mallozi *et al.* (1979), the wavelength spacing of the EXAFS peaks gave a nearest-neighbour distance of  $2.70 \text{ \AA}$  in the aluminium foil, which implies an actual distance of  $3.10 \text{ \AA}$ . Again this value is in approximate agreement with the known aluminium nearest-neighbour distance ( $2.86 \text{ \AA}$ ).

The crystal used in the Von Hamos spectrograph was PET, but we can expect a comparable diffraction efficiency (within a factor of 2, see Table 2) for EDDT used in the plane geometry spectrograph. Thus, the Von Hamos spectrograph is approximately an order of magnitude more sensitive than the plane crystal spectrograph once allowance is made for the different laser energies used in the single shot EXAFS exposures (required with the Von Hamos spectrograph) and the 50 laser shots (required with the plane crystal spectrograph). Mica crystals were also bent for the Von Hamos spectrograph, but were found to be unsuitable for recording EXAFS spectra because of the large number of diffraction orders which are superimposed on each exposure and which have comparable diffraction efficiencies.

## 4. Discussion

### (a) Model of X-ray Production

A simple model of X-ray production in our laser-produced plasma can be used to explain the observed variation of X-ray flux with parameters such as the laser energy (Fig. 3) and the position of the target relative to the laser focus (Fig. 4). The model can also be used to predict optimum conditions for X-ray emission. In order to develop the model, our observations that the plasma thermal temperature and the laser energy absorbed by the plasma vary minimally with laser intensity (Burgess *et al.* 1983; Perry 1986) are used as rationales for proposing that (i) the X-ray emission from the plasma is only proportional to the volume of heated plasma and that (ii) the thickness  $x$  of heated plasma increases linearly with laser energy  $E$ , i.e. the plasma self-regulates its heated volume in order to maintain the observed, constant temperature. We can write

$$x = x_0 E, \quad (1)$$

where  $x_0$  is the plasma thickness per unit laser energy. Ignoring the small effect due to a possible angle between the target normal and the laser axis, the variation of the laser

intensity  $I(r)$  on the target surface is assumed to be gaussian with radius  $r$ , that is

$$I(r) = I_0 \exp\{-(r/r_0)^2\}, \quad (2)$$

where  $I_0$  is the intensity on the laser axis. The scale-length  $r_0$  can be related, by using simple geometry, to the distance  $\Delta d$  between the target and the laser focus if diffraction and other effects as  $\Delta d \rightarrow 0$  are ignored. We have

$$r_0 = \frac{1}{2} C_f |\Delta d|, \quad (3)$$

where  $C_f$  is a factor determined by the laser focusing optics and the degree to which the laser beam fills the focusing lens. For the  $f/1$  laser focusing employed in our experiment,  $C_f \approx 0.75$ .

We now make an additional important assumption concerning the area of heated plasma at the target. The target material is assumed to be heated sufficiently for X-ray production only where the local laser intensity exceeds a threshold value  $I_t$ . This assumption would be valid, for example, if superthermal electrons dominate the heating of the thermal plasma (Burgess *et al.* 1984) as such a process could be expected to have a sharp intensity threshold. In any case, with our assumption, we can expect a hot, X-ray emitting plasma to be created for  $r < r_t$  where

$$r_t^2 = \frac{1}{4} C_f^2 (\Delta d)^2 \ln(I_0/I_t), \quad (4)$$

on using equations (2) and (3). For a laser pulse of energy  $E$  and duration  $\Delta t$  we can write

$$\begin{aligned} E/\Delta t &= \int_0^\infty 2\pi r I(r) dr \\ &= \frac{1}{4} \pi C_f^2 (\Delta d)^2 I_0, \end{aligned} \quad (5)$$

on substituting equations (2) and (3). Hence, the volume  $V$  of X-ray emitting plasma is

$$\begin{aligned} V &= x\pi r_t^2 \\ &= x_0 (E^2/\Delta t) I_0^{-1} \ln(I_0/I_t) \\ &= \frac{1}{4} \pi x_0 E C_f^2 (\Delta d)^2 \ln\{4E/\pi C_f^2 (\Delta d)^2 \Delta t I_t\}, \end{aligned} \quad (6)$$

by using equations (1), (4) and (5).

Variations of the X-ray flux from the laser-produced plasma are assumed to be proportional to the plasma volume and so expected X-ray flux variations obtained by equation (6) are plotted and compared with our experimental results in Figs 3–5. In these plots the threshold intensity which best fits the experimental results is set at  $I_t = 6 \times 10^{13} \text{ W cm}^{-2}$  and the same proportionality between the values of the X-ray flux detected and the plasma volume  $V$  given by equation (6) is used for each plot.

Experimentally measured values of the X-ray flux  $F$  as a function of laser energy  $E$  (Fig. 3) are well fitted with theoretical curves of the form of equation (6) for the two focusing positions (in-focus and defocused by  $150 \mu\text{m}$ ). The plasma volume for

the in-focus position (nominally  $\Delta d = 0$ ) is zero from equation (6), but clearly there is still a finite volume of hot plasma created when the target is at the laser focus position because of lateral thermal conduction, the lateral spread of superthermal electron heating and the fact that the laser focus has a finite, though small diameter (in our case  $\approx 2 \mu\text{m}$ ). Indeed, the ratio of X-ray flux in the defocused and in-focus target positions (Fig. 3) is particularly sensitive to an assumed value of  $\Delta d$  for the in-focus position and we may deduce from these results, using equation (6), that there is a minimum plasma diameter corresponding to  $\Delta d = 50 \pm 5 \mu\text{m}$ .

Values of experimentally measured X-ray flux  $F$  (normalized to a laser energy of 2 J) as a function of target position  $\Delta d$  (Fig. 4) are fitted reasonably well with curves of the form of equation (6). The effect of a minimum plasma size as  $\Delta d \rightarrow 0$  is shown by the broken curve in Fig. 4. The experimentally measured variation of X-ray production efficiency  $F/E$  as a function of laser intensity  $I$  (Fig. 5) is also approximately fitted with a curve of the form of equation (6). However, the experimental  $F/E$  points scatter about the theoretical curve because the  $F/E$  values vary linearly with laser energy according to equation (6), whereas the curve has been plotted under the assumption of a single constant value of  $E = 2.2 \text{ J}$ . Again, the effect of a minimum plasma size as  $\Delta d \rightarrow 0$  and the laser intensity  $I_0$  increases is shown by the broken curve in Fig. 5.

A variation of X-ray production efficiency with laser intensity similar to the variation we have measured (Fig. 5) has been explained by Lee and Ahlstrom (1984) in terms of a balance between energy loss due to ablation and thermal conduction into the solid target. This balance could cause a peak in X-ray production efficiency at intensities around  $2 \times 10^{14} \text{ W cm}^{-2}$ , as we have measured. However, the explanation offered by Lee and Ahlstrom (1984) cannot explain our observed variation of X-ray flux with laser energy and heuristically requires thermal conduction to decrease with increasing laser intensity over a very wide range of laser intensities (for  $I_0 > 10^{13} \text{ W cm}^{-2}$ ). This is not consistent with the data available on thermal conduction which suggests that the flux limiter is approximately constant at  $f \approx 0.03$  over our intensity range (Rosen 1984).

The X-ray emission model that we have developed in this subsection can be used to explain in a straightforward manner our observed increase in X-ray flux (for constant laser energy and focal position) by a factor of 3–4 when the laser wavelength  $\lambda_e$  is reduced from  $1.054$  to  $0.53 \mu\text{m}$ . The thickness  $x$  of the X-ray emitting plasma must decrease when the laser wavelength is lowered because the critical electron density (where the X-ray emission primarily occurs) increases and, in order to maintain a constant plasma temperature, the plasma volume must decrease. The critical electron density  $N_c$  is proportional to  $\lambda_e^{-2}$ , so the plasma thickness  $x$  is proportional to  $\lambda_e^2$ . It is well known that X-ray emission  $F$  for spectral lines, free-bound continuum and free-free continuum scales approximately with the electron density as  $F \propto N_e^2$  (see e.g. Griem 1964). Hence, allowing for the decrease in plasma volume with decreasing  $\lambda_e$ , we have  $F \propto x N_c^2 = \lambda_e^{-2}$  as observed.

#### (b) Efficiency of X-ray Production and Detection

The possibility of using a monojoule laser-based source for EXAFS studies can be judged from the results presented in Figs 3–6. Over a wavelength range of  $0.017 \text{ \AA}$  centred on  $4.8 \text{ \AA}$ , for example, the X-ray energy detected can readily be  $2 \times 10^{-10}$  that of the incident laser energy (Fig. 5). Taking account of the solid angle of collection

at this wavelength with our Von Hamos spectrograph ( $4 \times 10^{-3}$  sr), this gives an efficiency of conversion of laser energy into measurable X-ray energy (after detection) over a  $0.017 \text{ \AA}$  range at  $4.8 \text{ \AA}$  of  $3 \times 10^{-7}$ . Over a  $0.5 \text{ \AA}$  wavelength range, the efficiency is estimated to be  $10^{-5}$  of the incident laser energy. These efficiencies may seem to be small, but sensitive large aspect ratio silicon X-ray detectors can detect  $10^{-15}$  J of X-ray energy (Koppel 1976; Gamble *et al.* 1979). Using the example of an X-ray sensitive RETICON 1024 element line scanning array, which has elements  $12.5 \text{ \mu m}$  wide and 2 mm high (this geometry is ideal when collecting the X-ray flux from the focal region of a Von Hamos crystal), we can expect, when using a 50 mm radius PET crystal and a laser of energy 3 J, to obtain in the absence of a sample  $10^{-11}$  J per element at the detector plane. This represents a signal above the detection threshold by about  $10^4$ , an ample value for many applications. Further improvements in sensitivity (by about a factor of 5) may be obtained by utilizing pyrolytic graphite as the diffracting crystal (see Table 2). It is also possible to deposit pyrolytic graphite onto a cylindrical substrate and thus circumvent the problems of bending crystals to cylindrical shapes (Mead *et al.* 1972).

## 5. Conclusions

Continuum soft X-ray emission in the wavelength range from 3 to  $8 \text{ \AA}$  for a laser-produced plasma created by a short duration ( $\leq 150$  ps), low energy ( $\leq 6$  J per pulse) laser has been measured as a function of the laser energy, the position of the target relative to the laser focus, the target material, the laser pulse-length and the laser wavelength. The experimental results are well described by a simple model which relates the X-ray emission to the volume of hot plasma, while a recent alternative model of X-ray production (Lee and Ahlstrom 1984) has been shown to be inadequate to describe our experimental results (see Section 4a). Plane, cylindrical (Von Hamos) and elliptical X-ray spectrographs have all been investigated and it is shown that the Von Hamos spectrograph gives the most sensitive detection threshold for X-rays, while still providing high dispersion. Nevertheless the limited quality of cylindrically bent crystals significantly reduces the collection efficiency in this geometry when recording spectra on film.

By optimizing the X-ray emission from the plasma and the spectrograph sensitivity, single shot EXAFS spectra of aluminium have been produced by using the short duration, low energy laser-produced plasma as the X-ray source. It has been demonstrated that sufficient flux is available from a plasma generated by a monojoule short pulse ( $< 150$  ps) phosphate glass laser to record EXAFS spectra in the  $3\text{--}8 \text{ \AA}$  band, especially if improved detectors such as silicon line scanning arrays and highly efficient pyrolytic graphite diffracting crystals are employed. This result encourages the development of a new generation of compact high repetition rate, high power, pulsed lasers with this application in mind.

## Acknowledgments

We would like to acknowledge Dr M. G. Sceats (University of Sydney) for his advice and helpful supervision of one of us (M.A.H.) and to thank Dr N. H. Burnett (National Research Council, Canada) for helping with the production of cylindrically bent crystals. We also thank Mr G. Renner for his untiring efforts in constructing many of our pieces of apparatus and Mr A. J. Perry for making the absorption measurements.

## References

- Burgess, M. D. J., Dragila, R., and Luther-Davies, B. (1984). *Opt. Commun.* **52**, 189–94.
- Burgess, M. D. J., Dragila, R., Luther-Davies, B., Nugent, K. A., and Tallents, G. J. (1983). In 'Laser Interaction and Related Plasma Phenomena' (Eds H. Hora and G. H. Miley), pp. 463–78 (Plenum: New York).
- Busquet, M., Pain, D., Bauche, J., and Luc-Koenig, E. (1985). *Phys. Scr.* **31**, 137–48.
- Dozier, C. M., Brown, D. B., Binks, L. S., Lyons, P. B., and Benjamin, R. F. (1976). *J. Appl. Phys.* **47**, 3732–9.
- Eason, R. W., Bradley, D. K., Kilkeny, J. D., and Greaves, G. N. (1984). *J. Phys. C* **17**, 5067–74.
- Epstein, H. M., Schwerzel, R. E., and Campbell, B. E. (1983). In 'Laser Interaction and Related Plasma Phenomena' (Eds H. Hora and G. H. Miley), pp. 149–64 (Plenum: New York).
- Fontaine, A., Lagarde, P., Raoux, D., and Estava, J. M. (1979). *J. Phys. F* **9**, 2143–53.
- Forster, E., Goetz, K., Schafer, K., and Zimmer, W. D. (1984). *Laser Part. Beams* **2**, 167–85.
- Gamble, R. C., Baldeschwieler, J. D., and Giffin, C. E. (1979). *Rev. Scient. Instrum.* **50**, 1416–20.
- Germer, R. (1979). *J. Phys. E* **12**, 336–50.
- Gilfrich, J. V., Brown, D. B., and Burkhalter, P. G. (1975). *Appl. Spectrosc.* **29**, 322–6.
- Gould, R. W., Bates, S. R., and Sparks, C. J. (1968). *Appl. Spectrosc.* **22**, 549–51.
- Griem, H. (1964). 'Plasma Spectroscopy' (McGraw-Hill: New York).
- Henke, B. L., Yamada, H. T., and Tanaka, T. J. (1983). *Rev. Scient. Instrum.* **54**, 1311–30.
- Hohlfelder, J. J. (1974). *Adv. X Ray Anal.* **17**, 531–41.
- Kallne, E., Kallne, J., and Cowan, R. D. (1983). *Phys. Rev. A* **27**, 2682–97.
- Kiyokawa, S., Yabe, T., Miyanaga, N., Okada, K., Hasegawa, H., Mochizuki, T., Yamanaka, T., Yamanaka, C., and Kagawa, T. (1985). *Phys. Rev. Lett.* **54**, 1999–2002.
- Koppel, L. N. (1976). *Rev. Scient. Instrum.* **47**, 1109–12.
- Lee, P. H. Y., and Ahlstrom, H. G. (1984). *Laser Part. Beams* **2**, 303–7.
- Lewis, C. L. S., and Mahoney, E. R. (1984). *J. Phys. E* **17**, 744–6.
- Mallozi, P. J., Schwerzel, R. E., Epstein, H. M., and Campbell, B. E. (1979). *Science* **206**, 353–5.
- Mallozi, P. J., Schwerzel, R. E., Epstein, H. M., and Campbell, B. E. (1981). *Phys. Rev. A* **23**, 824–8.
- Mathews, D. L., Campbell, E. M., Ceglio, N. M., Hermes, G., Kauffman, R., Koppel, L., Lee, R., Manes, K., Rupert, V., Slivinsky, V. W., Turner, R., and Ze, F. (1983). *J. Appl. Phys.* **54**, 4260–8.
- Mead, S. W., Kidder, R. E., Swain, J. E., Ranier, F., and Petruzzzi, J. (1972). *Appl. Opt.* **11**, 345–52.
- Mead, W. C., *et al.* (1981). *Phys. Rev. Lett.* **47**, 1289–92.
- Mead, W. C., *et al.* (1983). *Phys. Fluids* **26**, 2316–31.
- Pendry, J. B. (1983). *Comments Solid State Phys.* **10**, 219–31.
- Perry, A. J. (1986). Ph.D. Thesis, Aust. National Univ.
- Rosen, M. D. (1984). *Comments Plasma Phys. Controlled Fusion* **8**, 165–75.
- Tallents, G. J., and Shorrock, L. D. (1981). *J. Phys. E* **14**, 20–3.
- Teo, B. (1980). *Acc. Chem. Res.* **13**, 412–9.
- Yaakobi, B., Bourke, P., Conturie, Y., Delettrez, J., Forsyth, J. M., Frankel, R. D., Goldman, L. M., McCrory, R. L., Seka, W., Soures, J. M., Burek, A. J., and Deslattes, R. E. (1981). *Opt. Commun.* **38**, 196–200.
- Yaakobi, B., and Burek, A. J. (1983). *IEEE J. Quantum Electron.* **QE 19**, 1841–54.
- Yaakobi, B., Turner, R. E., Schnopper, H. W., and Taylor, P. O. (1979). *Rev. Scient. Instrum.* **50**, 1609–11.